

Structural bioinformatics

# refineD: improved protein structure refinement using machine learning based restrained relaxation

Debswapna Bhattacharya  \*

Department of Computer Science and Software Engineering, Auburn University, Auburn, AL 36849, USA

\*To whom correspondence should be addressed.

Associate Editor: Alfonso Valencia

Received on June 13, 2018; revised on January 22, 2019; editorial decision on February 7, 2019; accepted on February 11, 2019

## Abstract

**Motivation:** Protein structure refinement aims to bring moderately accurate template-based protein models closer to the native state through conformational sampling. However, guiding the sampling towards the native state by effectively using restraints remains a major issue in structure refinement.

**Results:** Here, we develop a machine learning based restrained relaxation protocol that uses deep discriminative learning based binary classifiers to predict multi-resolution probabilistic restraints from the starting structure and subsequently converts these restraints to be integrated into Rosetta all-atom energy function as additional scoring terms during structure refinement. We use four restraint resolutions as adopted in GDT-HA (0.5, 1, 2 and 4 Å), centered on the C<sub>α</sub> atom of each residue that are predicted by ensemble of four deep discriminative classifiers trained using combinations of sequence and structure-derived features as well as several energy terms from Rosetta centroid scoring function. The proposed method, refineD, has been found to produce consistent and substantial structural refinement through the use of cumulative and non-cumulative restraints on 150 benchmarking targets. refineD outperforms unrestrained relaxation strategy or relaxation that is restrained to starting structures using the FastRelax application of Rosetta or atomic-level energy minimization based ModRefiner method as well as molecular dynamics (MD) simulation based FG-MD protocol. Furthermore, by adjusting restraint resolutions, the method addresses the tradeoff that exists between degree and consistency of refinement. These results demonstrate a promising new avenue for improving accuracy of template-based protein models by effectively guiding conformational sampling during structure refinement through the use of machine learning based restraints.

**Availability and implementation:** <http://watson.cse.eng.auburn.edu/refined/>.

**Contact:** [bhattacharyad@auburn.edu](mailto:bhattacharyad@auburn.edu)

**Supplementary information:** [Supplementary data](#) are available at *Bioinformatics* online.

## 1 Introduction

Computational protein structure prediction is an integral part of structural bioinformatics (Cavasotto and Phatak, 2009). The accuracy of protein models predicted by the state-of-the-art structure prediction approaches (Kim *et al.*, 2004; Rohl *et al.*, 2004; Zhang, 2008) can be quite impressive, particularly for the template-based

modeling cases (Kryshtafovych *et al.*, 2018; Moulton *et al.*, 2018). However, they still often fail to reach accuracy high enough to be comparable to the experimentally determined native conformations (Feig, 2017). The goal of computational protein structure refinement is to drive a starting structure towards its native state such that it attains near-experimental accuracy. Consequently, protein

structure refinement approaches use conformational sampling to optimize an atomistic force field to bring the starting structure closer to its native state.

The most successful refinement methods employ Molecular dynamics (MD) simulation (Feig and Mirjalili, 2016; Mirjalili *et al.*, 2014), Monte Carlo (MC) sampling (Bhattacharya and Cheng, 2013a, b, c; Park *et al.*, 2016; Park and Seok, 2012), energy minimization with a physics and/or knowledge based force fields (Bhattacharya and Cheng, 2013a, b, c; Bhattacharya *et al.*, 2016; Lee *et al.*, 2016; Lin *et al.*, 2011; Rodrigues *et al.*, 2012). Promising progress in structure refinement has been witnessed in the recent past due to force field improvement by combining physics and knowledge based scoring terms, enhanced sampling for longer time scales and the use of ensemble averaging (Hovan *et al.*, 2018; Modi and Dunbrack, 2016; Nugent *et al.*, 2014). Nevertheless, addressing the tradeoff between degree and consistency of refinement is a major challenge for state-of-the-art refinement protocols. On one hand, aggressive and unrestrained sampling around the starting structure that has the ability to produce large degree of refinement often deviates away from the native state rather than towards it (Park *et al.*, 2012; Summa and Levitt, 2007). On the other hand, applying restraints derived directly from the starting structure during refinement in order to prevent large conformational change (Chen and Brooks, 2007; Lee *et al.*, 2016; Raval *et al.*, 2012) opposes significant structural modifications that may be needed, particularly when the starting structure is far away from the native state. Some refinement approaches apply partial restraints on structurally conserved regions (Cao *et al.*, 2003; Ishitani *et al.*, 2008), or derive restraints using ensemble of homologues structure or fragments (Della Corte *et al.*, 2016; Wildberg *et al.*, 2015; Zhang *et al.*, 2011). However, effectively using restraints to achieve consistent yet significant refinement remains a conundrum in protein structure refinement (Feig, 2017; Heo and Feig, 2018).

Here, we present refined, which uses deep discriminative learning based ensemble classifiers to predict multi-resolution probabilistic restraints from the starting structure and subsequently converts these restraints into scoring terms to guide conformational sampling during structure refinement. Specifically, we use Deep Convolutional Neural Fields (DeepCNF) (Wang *et al.*, 2016a,b), a deep discriminative learning classifier, to predict the likelihood of  $C_\alpha$  atom of any residue of the starting structure to be within  $r$  Å with respect to the native. Following the high accuracy version of the Global Distance Test (GDT-HA) score (Zemla, 2003), which captures the number of residues in a predicted protein model with the  $C_\alpha$  atom distances from the corresponding residues in the native structure below four different distance thresholds (0.5, 1, 2, 4 Å) and extensively used to evaluate the performance of refinement methods, we use an ensemble of four DeepCNF classifiers after fixing  $r$  to each of the four distance thresholds. Each DeepCNF classifier combines several centroid scoring functions of Rosetta (Leaver-Fay *et al.*, 2011; Rohl *et al.*, 2004), sequence profile based residue conservation features and consistency between structural features extracted from the starting structure and predicted values from its sequence. Output from the ensemble of four DeepCNF classifiers are subsequently converted to multi-resolution probabilistic restraints and integrated as additional scoring term into Rosetta's all-atom energy function (Alford *et al.*, 2017) to perform restrained relaxation using the FastRelax application of Rosetta (Khatib *et al.*, 2011; Tyka *et al.*, 2011). To the best of our knowledge, this is the first study that applies machine learning derived multi-resolution probabilistic restraints in protein structure refinement.

## 2 Materials and methods

### 2.1 Training deep discriminative ensemble classifiers

#### 2.1.1 Training dataset

We use 3DRobot (Deng *et al.*, 2016) decoy set to curate dataset for training DeepCNF ensemble classifiers. 3DRobot generates well-packed decoy pool with an even distribution of decoy accuracy over the Root Mean Square Deviation (RMSD) space with respect to native. The original 3DRobot decoy set contains 200 non-homologous protein targets each with 300 decoys that are evenly distributed in the RMSD space from 0 to 12 Å. We compute GDT-HA score for each decoy in the 3DRobot dataset and group them into ten distinct GDT-HA bins with a bin-width of 10 GDT-HA units. For each target, we select at most one decoy from each bin by random sampling. This results in 1767 decoys for 200 targets. It should be noted that for few targets, not all ten GDT-HA bins are populated and this results in fewer than ten decoys being selected for that target.

#### 2.1.2 Feature generation

We use a total of fifteen features to describe each residue of a decoy as briefly described below.

- i. Sequence profile conservation score: We generate sequence profile by searching the NCBI non-redundant sequence database (NR) using three iterations of PSI-BLAST v2.2.26 software (Altschul *et al.*, 1997) with an E-value inclusion threshold of  $10^{-3}$ . We subsequently extract the information per position scores from the PSI-BLAST matrix and scale it between 0 and 1 using sigmoidal transformation. We use this scaled score as sequence profile conservation feature.
- ii. Consistency between predicted and observed structural properties: We use SPIDER2 (Heffernan *et al.*, 2015), an iterative deep learning framework, to predict secondary structure and absolute solvent accessibility from a given protein sequence. Observed secondary structure of a decoy is calculated using the DSSP (Kabsch and Sander, 1983) method implemented in PyRosetta (Chaudhury *et al.*, 2010). Per residue relative solvent accessible surface area of each residue is obtained using PyRosetta. We use a binary agreement between predicted and observed secondary structure as a feature. For solvent accessibility, we convert predicted absolute solvent accessibility into their corresponding relative values ( $rsa_p$ ) and compute squared error with respect to observed values ( $rsa_o$ ) as  $(rsa_p - rsa_o)^2$  to be used as a feature.
- iii. Rosetta centroid energy terms: We use twelve Rosetta centroid energy terms (Leaver-Fay *et al.*, 2011; Rohl *et al.*, 2004) including residue environment (env), residue pair interactions (pair),  $C\beta$  density (cbeta), steric repulsion (vdw), radius of gyration (rg), packing (cenpack), contact order (co), statistical potentials for secondary structure formation (hs\_pair, ss\_pair, sheet, rsigma) and centroid hydrogen-bonding (cen\_hb). Once again, we apply sigmoidal function to all terms to scale energy terms before incorporating them as features.

#### 2.1.3 Label generation

We set the class label as 1 (a.k.a. positive class) if the  $C_\alpha$  atom of a residue is within  $r$  Å with respect to the native structure after optimal structural superposition and 0 (a.k.a. negative class) otherwise. Four different class labels are generated after fixing  $r$  at 0.5, 1, 2, 4 Å respectively. It should be noted here that class labels at lower distance thresholds always agree with that of their higher distance counterparts, but the converse may not be true. Moreover,

depending on the accuracy of the decoy and the choice of the distance thresholds, one class may vastly outnumber the other; resulting in a class imbalance problem. In the training dataset, ratios between positive and negative classes are 0.21 (40 849/194 621), 0.51 (78 755/156 715), 1.05 (120 334/115 136) and 2.31 (164 421/ 71 049) at distance thresholds 0.5, 1, 2 and 4 Å respectively. Class imbalance problem is, therefore, particularly noticeable for the low- and highest distance thresholds.

### 2.1.4 Architecture and parameters of deep discriminative classifiers

The architecture of deep discriminative classifier, DeepCNF (Wang *et al.*, 2016a,b) that is particularly suited for learning from imbalanced datasets, consists of two modules: (i) the Conditional Random Fields (CRF) module covering the top layer and the class label layer, and (ii) the deep convolutional neural network (DCNN) module covering the input to the top layer. DeepCNF strives to address class imbalance problem in the training data by maximizing the empirical Area Under the ROC Curve (AUC), which is an unbiased measurement for imbalanced data. Based on preliminary testing, we use 5 hidden layers each having 50 neurons with a window size of 21 and a sigmoid activation function for all four DeepCNF classifiers. All four classifiers use the same feature set but different class labels corresponding to distance cutoffs 0.5, 1, 2, 4 Å. Based on preliminary testing, we set the regularizer to 0.5, number of iterations to 1000, AUC degree to 3 and uniform weights defaulted to 1.0 for each labels. A thorough parameter optimization may help further improve the performance.

## 2.2 refinedD protocol

The flowchart of refinedD protocol is shown in Figure 1, which consists of feature generation from the starting structure, residue level ensemble classification using the trained DeepCNF classifiers, multi-resolution probabilistic restraints generation, structure refinement via restrained relaxation, and scoring refined structures.

### 2.2.1 Feature generation from the starting structure

Given a starting structure for refinement, we extract the previously mentioned set of fifteen features that includes: (i) one feature representing sequence profile conservation score; (ii) two features quantifying the consistency between predicted and observed structural

properties (secondary structure and solvent accessibility); and (iii) twelve Rosetta centroid energy terms.

### 2.2.2 Residue level ensemble classifications

Based on the features derived from the starting structure and using one of the four DeepCNF classifiers trained on class labels generated using a specific distance threshold  $r$  Å, we can classify residue  $i$  in the starting structure to be within  $r$  Å compared to the native structure, where  $r \in \{0.5, 1, 2, 4\}$  Å. Collectively, the four trained DeepCNF classifiers result in residue level ensemble classification.

### 2.2.3 Generating multi-resolution probabilistic restraints

We convert residue level ensemble classifications to multi-resolution probabilistic restraints based on four distance thresholds  $r \in \{0.5, 1, 2, 4\}$  Å. Specifically, we apply Rosetta CoordinateConstraint on each of the  $C_\alpha$  atom of the starting structure weighted by their associated probabilities after employing FLAT\_HARMONIC function to integrate into the full atom Rosetta Energy Function 2015 (REF15) (Alford *et al.*, 2017). FLAT\_HARMONIC is a harmonic potential split at  $x_0$  with a  $2 * tol$  length region of zero inserted (i.e. zero in the range of  $x_0 - tol$  to  $x_0 + tol$ ). Outside the range, it is harmonic function with width parameter  $sd$ :

$$f(x) = \left( \frac{x - x_0}{sd} \right)^2$$

We fix  $x_0$  at zero and set the  $tol$  parameter to each of the four distance thresholds  $r \in \{0.5, 1, 2, 4\}$  Å to allow unrestricted sampling guided purely by the REF15 scoring function in a spherical conformational space of radius  $r$  Å centered at each  $C_\alpha$  atom of the starting structure. Outside this region, conformational sampling is harmonically restricted using a width parameter  $sd$  of 0.1. Consequently, this corresponds to probabilistically restraining the conformational space at four different resolutions.

### 2.2.4 Structure refinement via restrained relaxation

We use the FastRelax application of Rosetta (Khatib *et al.*, 2011; Tyka *et al.*, 2011) accessed from PyRosetta (Chaudhury *et al.*, 2010) after setting the score function weights to ref2015\_cst.wts, which adds restraints based terms with the standard REF15 score function. The FastRelax protocol employs multiple rounds of repulsive weight annealing together with combinatorial rotamer optimization and minimization (ramp-repack-min). There are five cycles each consisting of four rounds of ramp-repack-min, where the strength of the repulsive energy term is progressively increased starting from 2% of full strength, followed by 25, 55 and 100%.

### 2.2.5 Scoring refined structures using ensemble classifiers

A refined structure produced through restrained relaxation can be assigned an accuracy score by combining residue level ensemble classifications in a weighted fashion analogous to GDT-HA score:

$$score = \frac{\sum_{r \in \{0.5, 1, 2, 4\}} \sum_{i=1}^L P(d_i \leq r | m_r)}{4L}$$

where  $P(d_i \leq r | m_r)$  is the probability of residue  $i$  in a refined structure to be within  $r$  Å compared to the native structure as predicted by DeepCNF classifier  $m_r$  trained on class labels generated using distance thresholds  $r$  Å. If the total probability mass at lower distance thresholds exceeds that for higher distance thresholds, we truncate the total probability mass for lower distance to that of higher

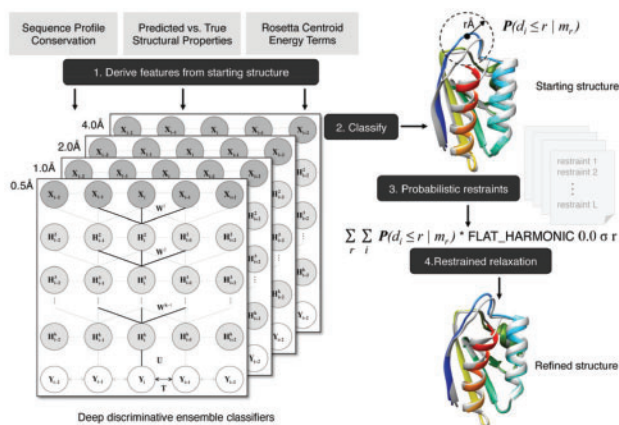


**Fig. 1.** Flowchart of the refinedD protocol. The protocol includes feature generation from the starting structure, residue level ensemble classification, multi-resolution probabilistic restraints generation, structure refinement via restrained relax, and scoring refined structures using ensemble classifiers

distance thresholds. The rationale for this is to mimic GDT-HA score, where number of aligned residues at lower distance thresholds is no greater than that at higher distance thresholds. Consequently, the accuracy score lies between [0, 1] with higher value indicating better accuracy.

### 3 Results and discussions

#### 3.1 Benchmark dataset

We collect a dataset comprising of 181 non-redundant single-domain proteins, originally curated to benchmark the FG-MD refinement protocol (Zhang *et al.*, 2011) spanning across multiple folds. We remove protein targets having significant sequence similarity with the training set. After removal of 31 such targets from the original FG-MD set, our benchmark dataset consists of 150 targets, with average sequence identity of 18.5% (maximum 25.2%) between the test and training set and length varying from 64 to 222 residues. For each protein target, the starting structure for refinement is generated by I-TASSER (Roy *et al.*, 2010; Zhang, 2007) using a multiple template based protein structure prediction approach. As shown in Figure 2A, 28% (42/150) targets have GDT-HA score of the starting structures below 40, 42.67% (64/150) targets with starting GDT-HA scores between 40 and 60, and 29.33% (44/150) targets have starting GDT-HA scores above 60.

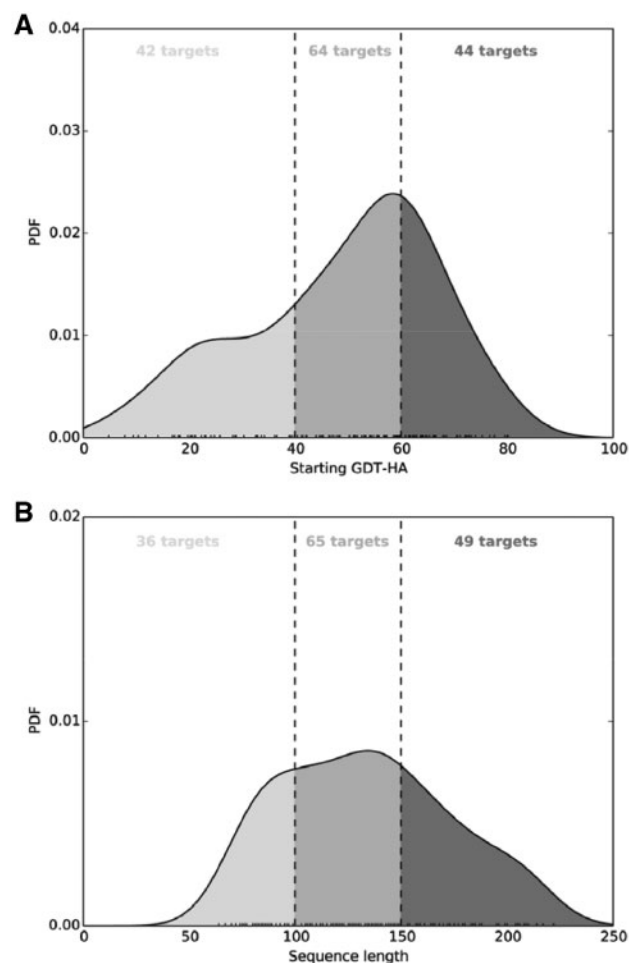


**Fig. 2.** Normalized probability distributions of target accuracy and length of the benchmark dataset. (A) GDT-HA scores of the starting structures; (B) sequence length

Additionally, Figure 2B shows that 24% (36/150) targets have length less than 100 residues, 43.33% (65/150) targets with length between 100 and 150 residues, and 32.67% (49/150) targets have length greater than 150 residues. The dataset, therefore, is diversely distributed in terms of accuracy of the starting structures as well as sequence lengths.

#### 3.2 Effects of multi-resolution probabilistic restraints

To investigate the effects of applying multi-resolution probabilistic restraints in structure refinement, we perform four distinct restrained relaxation runs for all 150 targets in the benchmark dataset. Each restraint relaxation run uses a specific restraint resolution corresponding to one of the four distance thresholds  $r \in \{0.5, 1, 2, 4\}$  Å and generates one set of refined structures. In Table 1, we show GDT-HA score of the refined structures generated using different restraint resolutions along with the starting GDT-HA score averaged over the entire dataset (Supplementary Table S1). On an average, only using restraints at 0.5 Å resolution results in net positive refinement with 57.33% (86/150) rate of successful refinement; while restraints at 1, 2 and 4 Å resolutions results in overall negative refinement with gradually decreasing successful refinement rate of 46% (69/150), 30% (45/150) and 24.67% (37/150) respectively. In terms of the average  $\Delta$ GDT-HA, minor increase (0.5425) for 0.5 Å restraints and minor decrease (−0.0422) for 1 Å restraints has been observed, while 2 and 4 Å restraints produce substantial structural degradation (−1.3942 and −2.7407 respectively). The average GDT-HA score of the refined models, therefore, steadily declines as restraint resolutions vary from 0.5 to 4 Å.

In Figure 3, we show the normalized probability distributions of the score changes ( $\Delta$ GDT-HA) at various restraint resolutions for the entire benchmark set. The results further demonstrate that the median score change gradually shifts towards the negative  $\Delta$ GDT-HA realm as restraint resolution moves from 0.5 to 4 Å. Prevalence of conservative structural modifications with  $\Delta$ GDT-HA ranging between −5 and 5 units are observed at 0.5 and 1 Å resolutions, while adventurous degree of conformational change of 5 or more GDT-HA units can be observed at 2 and 4 Å resolutions albeit at the expense of increased likelihood of worsening the starting structure. Even with enhanced potential of structural worsening at 2 and 4 Å resolutions with 18.7 and 31.3% of starting structures taking a loss of 5 or more GDT-HA units respectively, 6 and 4.7% cases show remarkable examples of refinement improving the starting structures by 5–20 GDT-HA units. The results indicate that the choice of restraint resolution is closely related to the tradeoff between degree and consistency of refinement. Restraint resolutions of 0.5 and 1 Å result in modest yet consistent refinement while 2 and 4 Å restraint

**Table 1.** Average GDT-HA score after refinement using different restraint resolutions in a benchmark set of 150 targets

Restraint resolution	Avg. GDT-HA <sup>a</sup> (Avg. $\Delta$ GDT-HA <sup>b</sup> )
0.5 Å restraints	49.5413 (0.5425)
Null <sup>c</sup>	48.9988 (0.0)
1.0 Å restraints	48.9566 (−0.0422)
2.0 Å restraints	47.6046 (−1.3942)
4.0 Å restraints	46.2581 (−2.7407)

<sup>a</sup>GDT-HA values are sorted in non-increasing order.

<sup>b</sup>Values in parenthesis are difference between average refined GDT-HA for each restraint type and the average starting GDT-HA. A positive number indicates successful refinement on an average.

<sup>c</sup>Represents the starting structures.

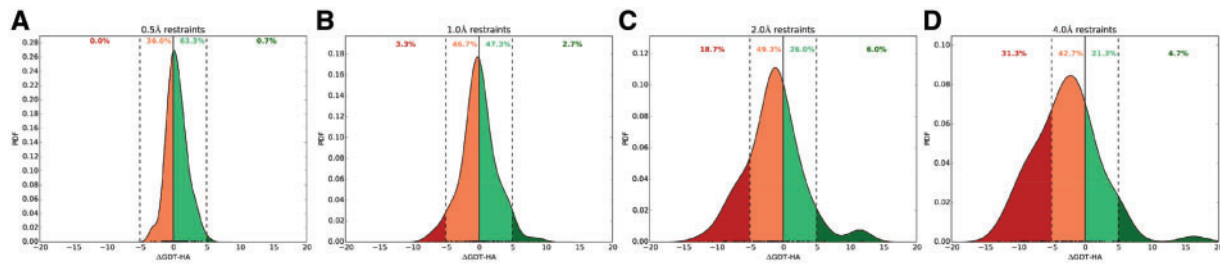


**Fig. 3.** Effect of multi-resolution probabilistic restraints on degree of structural change. Normalized probability density function (PDF) distributions of GDT-HA differences between the refined and starting structures over all 150 benchmark proteins using restrained relaxation with probabilistic restraints at (A) 0.5 Å; (B) 1 Å; (C) 2 Å; (D) 4 Å. Numbers indicate % of refined structures belonging to different  $\Delta$ GDT-HA ranges

resolutions have the potential to make substantial degree of refinement but often at the expense of consistency.

### 3.3 Refinement with cumulative and non-cumulative restraints

Given the starting structure, we use DeepCNF classifiers for residue level ensemble classification to generate multi-resolution probabilistic restraints and cumulatively integrate them into REF15 scoring function of Rosetta. Consequently, all restraints are simultaneously applied for all residues weighted according to their probabilities as predicted by ensemble of DeepCNF classifiers. We iteratively apply restrained FastRelax protocol for five iterations using four parallel threads to generate a total of twenty refined models. We subsequently apply the ensemble classifier based scoring function described above to score the resulting twenty refined structures and select the five top high scoring refined structures. This corresponds to employing refinedD with cumulative restraints (hereafter called refinedD-C). We also develop an alternative refinement strategy by using DeepCNF classifiers for residue level ensemble classification to generate multi-resolution probabilistic restraints and integrate them into REF15 scoring function of Rosetta in a non-cumulative way. That is, each multi-resolution restraint is individually applied for all residues weighted according to their probabilities as predicted by ensemble of DeepCNF classifiers. Once again, we apply restrained FastRelax protocol for five iterations using four parallel threads to generate a total of twenty refined models, but this time each parallel thread uses different restraint resolution. We subsequently apply the previously described scoring function to score the resulting twenty refined structures and select the top five high scoring refined structures. This corresponds to employing refinedD with non-cumulative restraints (hereafter called refinedD-NC). As controls, we employ FastRelax without any restraints as well as four sets of FastRelax runs after applying Rosetta CoordinateConstraint on each of the  $C_\alpha$  atom of the starting structure with FLAT\_HARMONIC restraints of 0.5, 1, 2, 4 Å having uniform restraint weights of 1.0 (hereafter called FastRelax- $r$  Å,  $r \in \{0.5, 1, 2, 4\}$  Å), as opposed to the probabilistically weighted restraints predicted by ensemble of DeepCNF classifiers. We generate twenty refined structures per target for each FastRelax- $r$  Å run and subsequently use Rosetta Energy Function 2015 (REF15) to select five refined structures having lowest REF15 energy values. Additionally, we refine the starting structures using two widely used refinement methods FG-MD (Zhang *et al.*, 2011) and ModRefiner (Xu and Zhang, 2011). FG-MD applies fragment-guided MD simulation while ModRefiner relies on atomic-level energy minimization. For FG-MD, we collect the refined structures directly from <https://zhanglab.cmb.med.umich.edu/FG-MD/>. We perform two sets of ModRefiner runs: (i) using a strength of 0 for the pairwise  $C_\alpha$  based distance restraints derived from the starting

structures (ModRefiner-0); and (ii) using a strength of 100 for the pairwise  $C_\alpha$  based distance restraints derived from the starting structures (ModRefiner-100). This results in two sets of refined conformations for the benchmark set. It should be noted that restraint strength 0 in ModRefiner represents unrestrained refinement allowing large conformational change, while restraint strength 100 in ModRefiner restricts substantial structural modification. In Table 2, we show average  $\Delta$ GDT-HA of the refined structures as well as  $P$ -values of Wilcoxon signed-rank test with the null hypothesis that refined structures produced by refinement are same as starting structures. Figure 4 shows the distributions of the score changes ( $\Delta$ GDT-HA) for refined against the controls (Supplementary Tables S2–S3).

The results demonstrate that out of the ten refinement protocols tested, only three (refinedD-C, FG-MD and ModRefiner-100) produce overall positive refinement as indicated by a positive average  $\Delta$ GDT-HA score considering the top 1 refined structure, even though the degree of refinement is modest in nature. refinedD-NC, FastRelax, FastRelax-0.5 Å, FastRelax-1.0 Å, FastRelax-2.0 Å, FastRelax-4.0 Å as well as ModRefiner-0 refinements result in overall negative refinement. ModRefiner-100, despite showing overall positive refinement, is not statistically significant at 95% confidence level as revealed by Wilcoxon Signed Rank Test. refinedD-C and FG-MD produces statistically significant refinement at 95% confidence level, with refinedD-C having the highest  $\Delta$ GDT-HA score. It should be noted here that FG-MD uses homologous fragment derived restraint information during refinement to guide MD simulations. refinedD-C, on the other hand, is based purely on machine learning derived restrained relaxation completely free from homology. Better performance of homology-free method such as refinedD-C makes it suitable for refining protein targets irrespective of homology. Performance of refinedD-C is statistically significantly better at 95% confidence level compared to the controls as revealed by one-sample t-test of the GDT-HA score differences between the refined structures produced by refinedD-C and controls ( $P$ -values of  $1.459 \times 10^{-16}$ ,  $6.69374 \times 10^{-20}$ ,  $9.55371 \times 10^{-8}$ ,  $1.29607 \times 10^{-7}$  and  $1.14242 \times 10^{-11}$  for FastRelax, FastRelax-0.5 Å, FastRelax-1.0 Å, FastRelax-2.0 Å and FastRelax-4.0 Å respectively). refinedD-C is also much more consistent than the controls in terms of number of successful refinement cases ( $\Delta$ GDT-HA score  $> 0$ ) achieving 63% (94/150) success while FastRelax, FastRelax-0.5 Å, FastRelax-1.0 Å, FastRelax-2.0 Å and FastRelax-4.0 Å attaining 20% (30/150), 37% (55/150), 43% (64/150), 33% (50/150) and 27% (41/150) successes respectively. refinedD-NC, while not as consistent as refinedD-C, attains 38% (57/150) success that is similar to that of FastRelax-0.5 Å. In terms of best of top 5 refined structures, refinedD-NC, refinedD-C, FastRelax-0.5 Å, FastRelax-1.0 Å, FastRelax-2.0 Å and FastRelax-4.0 Å refinements result in overall positive refinement with refinedD-NC attaining the highest average  $\Delta$ GDT-HA score.

**Table 2.** Comparison between refinedD with cumulative and non-cumulative restraints and other refinement methods based on average  $\Delta$ GDT-HA score in a benchmark set of 150 targets

Method	Avg. $\Delta$ top 1 <sup>a</sup> ( <i>P</i> -value <sup>b</sup> )	Avg. $\Delta$ best of 5 <sup>c</sup> ( <i>P</i> -value)
refinedD-C <sup>d</sup>	<b>0.6365</b> ( $7.11606 \times 10^{-7}$ )	1.3109 ( $8.24092 \times 10^{-18}$ )
refinedD-NC <sup>e</sup>	-1.2403 (0.000302906)	<b>1.5343</b> ( $1.45904 \times 10^{-8}$ )
FG-MD	0.5597 ( $1.34714 \times 10^{-7}$ )	0.5597 ( $1.34714 \times 10^{-7}$ )
FastRelax	-3.4317 ( $2.24913 \times 10^{-12}$ )	-0.1999 (0.61376)
FastRelax-0.5 Å	-0.1403 (0.03498)	0.0548 (0.853297)
FastRelax-1.0 Å	-0.3411 (0.082146)	0.8811 (0.0000328637)
FastRelax-2.0 Å	-1.2120 (0.000044333)	0.8223 (0.117838)
FastRelax-4.0 Å	-2.5471 ( $7.39414 \times 10^{-9}$ )	0.0751 (0.561429)
ModRefiner-0 <sup>f</sup>	-0.8400 (0.00268802)	-0.8400 (0.00268802)
ModRefiner-100 <sup>g</sup>	0.1491 (0.0675135)	0.1491 (0.0675135)

Note: Bold numbers indicate best in each category.

<sup>a</sup>Average  $\Delta$ GDT-HA of top selected model. Positive number indicates successful refinement.

<sup>b</sup>*P*-value of Wilcoxon Signed Rank Test.

<sup>c</sup>Average  $\Delta$ GDT-HA of the best of top five selected models.

<sup>d</sup>refinedD with cumulative restraints.

<sup>e</sup>refinedD with non-cumulative restraints.

<sup>f</sup>ModRefiner with strength of starting structure derived restraints set to 0.

<sup>g</sup>ModRefiner with strength of starting structure derived restraints set to 100.

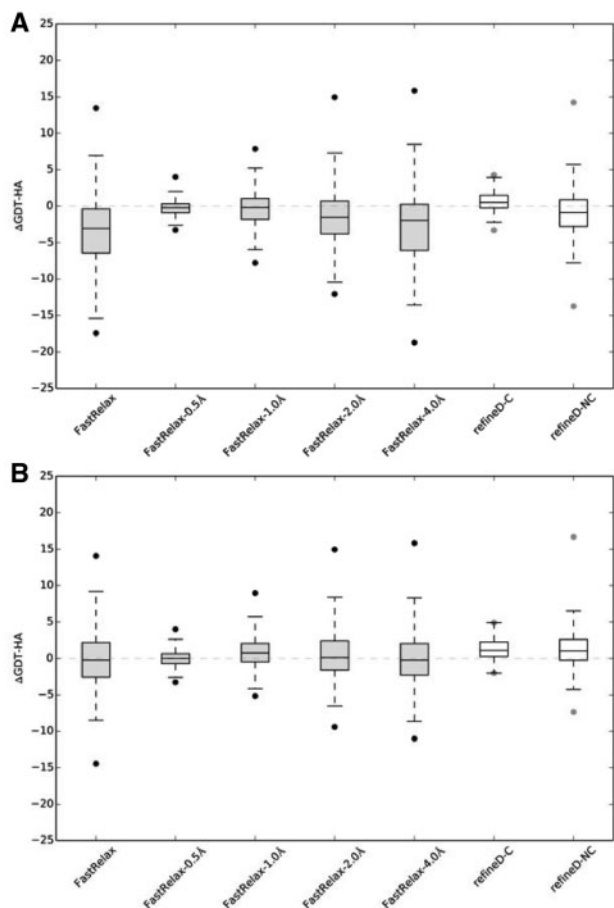


**Fig. 4.** Refinement degree distributions for refinedD against controls.  $\Delta$ GDT-HA distributions over all 150 benchmark proteins considering (A) top 1 refined structure; (B) best of top 5 refined structures

However, only refinedD-NC, refinedD-C and FastRelax-1.0 Å refinements are statistically significant at 95% confidence level as revealed by Wilcoxon Signed Rank Test. Performance differences of refinedD-NC are statistically significantly better than the controls (*P*-values of

one-sample *t*-tests are  $3.25713 \times 10^{-7}$ ,  $4.44823 \times 10^{-10}$ ,  $0.000533175$ ,  $0.000590979$  and  $3.25617 \times 10^{-7}$  for FastRelax, FastRelax-0.5 Å, FastRelax-1.0 Å, FastRelax-2.0 Å and FastRelax-4.0 Å respectively). Except for FastRelax-1.0 Å, refinedD-C also delivers statistically significantly better performance compared to the controls (*P*-values of one-sample *t*-tests are  $0.0002796$ ,  $1.04138 \times 10^{-42}$ ,  $0.00604323$  and  $0.00112333$  for FastRelax, FastRelax-0.5 Å, FastRelax-2.0 Å and FastRelax-4.0 Å respectively). Once again, refinedD-C attains most consistent refinement with 81% (121/150) success followed by refinedD-NC 69% (104/150), better than the controls with 40% (70/150), 43% (64/150), 60% (90/150), 51% (77/150) and 45% (67/150) successes for FastRelax, FastRelax-0.5 Å, FastRelax-1.0 Å, FastRelax-2.0 Å and FastRelax-4.0 Å respectively. Overall, the results indicate that refinedD-C corresponds to a conservative refinement strategy achieving consistent but modest refinement that is statistically significant. refinedD-NC, on the other hand, is an adventurous refinement strategy capable of making significant and pronounced degree of refinement.

Some representative examples of pronounced refinement with refinedD-NC are shown in Figure 5. Protein targets 1x6iA (Fig. 5A) and 2o37A (Fig. 5B) are primarily  $\alpha$ -helical in nature with the GDT-HA score of the corresponding starting structures around 55. Refinement for these targets results in 29.99 and 18.32% improvements in GDT-HA scores respectively, bringing the refined GDT-HA scores of these proteins to values greater than 65. Refinement for targets 2pv2A (Fig. 5C) and 3cjsB (Fig. 5D) with mixed  $\alpha$ -helical and  $\beta$ -sheet geometries improve GDT-HA scores by 15.31 and 29.1% respectively. In all cases, structural improvements are distributed across the entire chain causing a substantial global refinement of the starting structures.

### 3.4 Impact of enhanced sampling and alternative scoring

To investigate whether enhanced sampling and alternative scoring affect the performance of cumulative and non-cumulative refinedD methods, we conduct twofold experiments via: (i) 5-fold enhancement in sampling compared to the original pool of 20 refined structures by applying restrained relaxation runs for twenty five iterations using four parallel threads to generated 100 refined

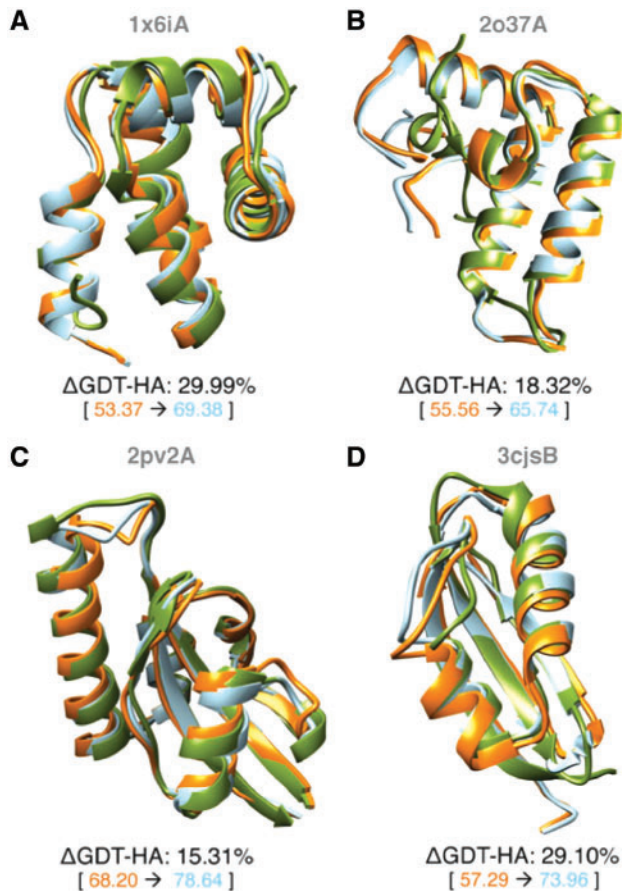


**Fig. 5.** Representative examples of refineD-NC refinement. For each example shown in (A–D), the starting (orange) and refined (cyan) structures are overlaid on the experimental (green) structures with numeric degrees of refinement shown below

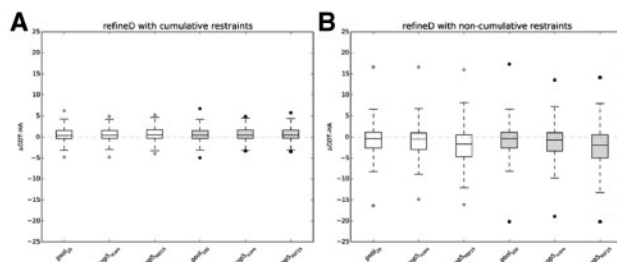


**Fig. 6.** Impact of enhanced sampling and alternative scoring.  $\Delta\text{GDT-HA}$  distributions over all 150 benchmark proteins for pools of original ( $\text{pool}_{20}$ ) and enhanced ( $\text{pool}_{100}$ ) sampling and top five refined structures selected using ensemble classifier based scoring function ( $\text{top5}_{\text{score}}$ ) and REF15 ( $\text{top5}_{\text{REF15}}$ ) for (A) refinedD with cumulative restraints; (B) refinedD with non-cumulative restraints

structures for all 150 targets in the benchmark dataset; and (ii) using the full atom Rosetta Energy Function 2015 (REF15) for selecting top five high scoring refined structures from the pools of original ( $\text{pool}_{20}$ ) and enhanced ( $\text{pool}_{100}$ ) sampling.

In Figure 6, we show the distributions of  $\Delta\text{GDT-HA}$  for  $\text{pool}_{20}$  and  $\text{pool}_{100}$  as well as top 5 refined structures selected by REF15 and ensemble classifier based scoring function for both cumulative and non-cumulative refinedD methods. For relaxation with cumulative restraints, the average  $\Delta\text{GDT-HA}$  is  $-0.85$  for  $\text{pool}_{20}$ , slightly

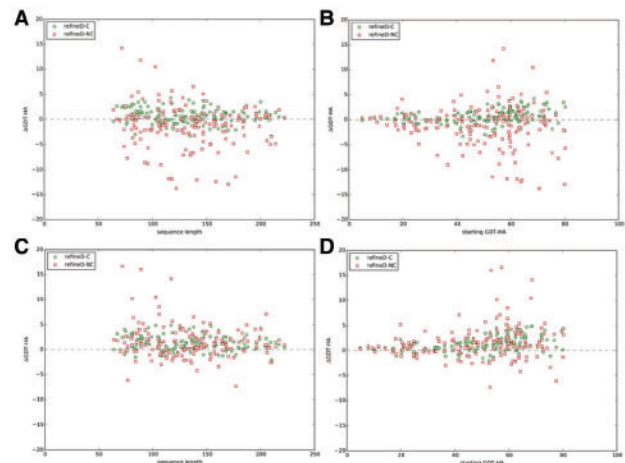


**Fig. 7.** Lengths and accuracies of starting structures against degree of structural refinement.  $\Delta\text{GDT-HA}$  scores against length (A), (C) and GDT-HA of the starting structures (B), (D) over all 150 benchmark proteins for refineD-C and refineD-NC methods for top 1 (A), (B) and the best of top 5 (C), (D) refined structures selected using ensemble classifier based scoring function

better compared to the average  $\Delta\text{GDT-HA}$  of  $-0.88$  for  $\text{pool}_{100}$ . The average  $\Delta\text{GDT-HA}$  of top 5 refined structures selected by ensemble classifier based scoring function from  $\text{pool}_{20}$  is  $-1.07$ , while selection from  $\text{pool}_{20}$  using REF15 degrades the performance compared to the ensemble classifier based scoring function with an average of  $-2.0$   $\Delta\text{GDT-HA}$  points. For  $\text{pool}_{100}$ , REF15 selection degrades the average from  $-1.32$  to  $-2.16$ . For relaxation with non-cumulative restraints, the averages for  $\text{pool}_{20}$  and  $\text{pool}_{100}$  are comparable with  $\Delta\text{GDT-HA}$  values of around  $0.6$ . In this case, REF15 selection outperforms the ensemble classifier based scoring function with an average of  $0.73$  compared to  $0.61$  for  $\text{pool}_{20}$ , and  $0.68$  compared to  $0.63$  for  $\text{pool}_{100}$ . Collectively, the results indicate that enhanced sampling or alternative scoring may offer slight performance improvement for refinedD with non-cumulative restraints.

### 3.5 Relationships between degree of structural refinement and nature of the starting structures

Figure 7 shows the lengths of the starting structures and GDT-HA scores of the starting structures against  $\Delta\text{GDT-HA}$  values for both refinedD-C and refinedD-NC methods in terms of top 1 and the best of top 5 refined structures selected by ensemble classifier based scoring function. Overall, the degree of refinement is noticeable for smaller targets (length  $< 100$  residues) and medium range of starting GDT-HA scores ( $40 < \text{GDT-HA} < 60$ ). This trend gets amplified for the best of top 5 compared to top 1 refined structure, particularly for refinedD-NC.

In Figure 8, we show the degree of structural refinement measured in term of  $\Delta\text{GDT-HA}$  scores of the best of top five refined structures using refinedD-NC with respect to the accuracy of the corresponding starting structures (in terms of GDT-HA) for targets of different lengths (Fig. 8A–C) and different accuracies of starting structures (Fig. 8D–F). Once again, the best improvement is observed for smaller targets having length less than 100 residues with 16.7% of starting structures showing remarkable examples of refinement by improving the starting structures by 5–20 GDT-HA units (Fig. 8A) and those in the medium range of starting accuracies having starting GDT-HA scores between 40 and 60 units with 15.6% cases making marked positive refinement of 5 or more GDT-HA units (Fig. 8E). We additionally examine whether the refinement

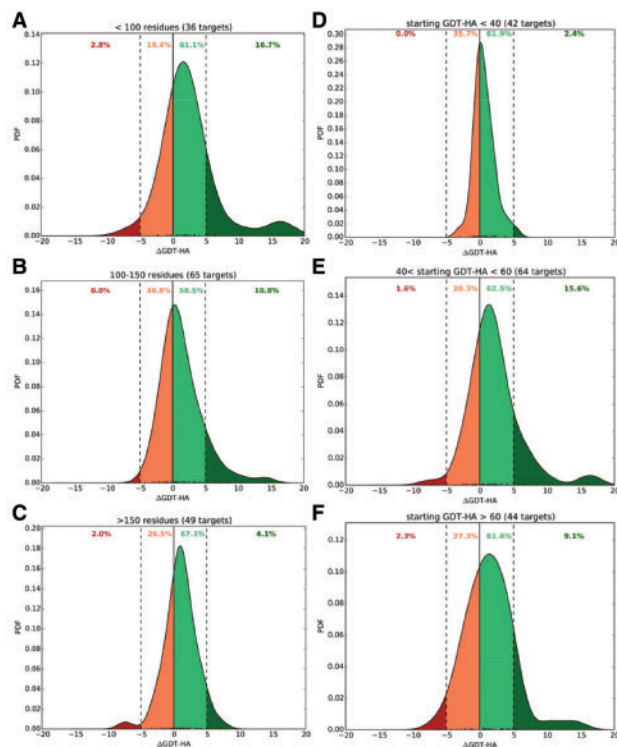


**Fig. 8.** Degree of refinement of refineD-NC for different target lengths and different starting GDT-HA. Normalized probability density function (PDF) distributions of  $\Delta$ GDT-HA scores for different target length bins (A–C) and different starting GDT-HA bins (D–F). Data for the best of top 5 refined structures presented

performance is affected when a test protein shares the same family, superfamily and fold similarity with any of the 200 proteins in the training dataset (Supplementary Fig. S1).

## 4 Conclusions

To use or not to use restraints during protein structure refinement remains a conundrum (Feig, 2017; Heo and Feig, 2018). We develop a novel refinement method called refineD, which uses deep discriminative learning based ensemble classifiers to predict multi-resolution probabilistic restraints from the starting structure and converts these restraints into scoring terms to guide conformational sampling during structure refinement and subsequently scores a pool of resulting refined structures using ensemble classifier based scoring. For the first time, we demonstrate that machine learning based restrained relaxation is able to address the tradeoff that exists between degree and consistency of refinement. refineD is shown to produce consistent and aggressive structural refinement through the use of cumulative and non-cumulative restraints. We demonstrate that the resolution of restraint directly affects the degree of conformational change that can be used for conservative or adventurous structure refinement. Compared to unrestrained relaxation or relaxation restrained to starting structures using the FastRelax application of Rosetta or atomic-level energy minimization based ModRefiner method, refineD delivers better performance in terms of consistency and substantial structural refinement. Moreover, homology-free refineD method outperforms MD simulation based FG-MD protocol, which uses homologous information. Collectively, these results demonstrate a promising new direction in protein structure refinement by using machine learning based

restraints to drive moderately accurate template-based protein models closer to the native state, making refineD an useful contribution in the field of protein structure prediction in particular and protein structural bioinformatics in general.

## Acknowledgements

The author wants to thank Md Hossain Shuvo and Sutanu Bhattacharya for helpful discussions.

## Funding

The work was partially supported by an Auburn University new faculty start-up grant to DB.

*Conflict of Interest:* none declared.

## References

- Alford, R.F. *et al.* (2017) The Rosetta all-atom energy function for macromolecular modeling and design. *J. Chem. Theory Comput.*, **13**, 3031–3048.
- Altschul, S.F. *et al.* (1997) Gapped BLAST and PSI-BLAST: a new generation of protein database search programs. *Nucleic Acids Res.*, **25**, 3389–3402.
- Bhattacharya, D. and Cheng, J. (2013a) 3Drefine: consistent protein structure refinement by optimizing hydrogen bonding network and atomic-level energy minimization. *Proteins Struct. Funct. Bioinf.*, **81**, 119–131.
- Bhattacharya, D. and Cheng, J. (2013b) i3Drefine software for protein 3D structure refinement and its assessment in CASP10. *PLoS One*, **8**, e69648.
- Bhattacharya, D. and Cheng, J. (2013c) Protein structure refinement by iterative fragment exchange. In: *Proceedings of the International Conference on Bioinformatics, Computational Biology and Biomedical Informatics*. ACM, p. 106.
- Bhattacharya, D. *et al.* (2016) 3Drefine: an interactive web server for efficient protein structure refinement. *Nucleic Acids Res.*, **44**, W406–W409.
- Cao, W. *et al.* (2003) Refinement of comparative-modeling structures by multicanonical molecular dynamics. *Genome Inf.*, **14**, 484–485.
- Cavasotto, C.N. and Phatak, S.S. (2009) Homology modeling in drug discovery: current trends and applications. *Drug Disc. Today*, **14**, 676–683.
- Chaudhury, S. *et al.* (2010) PyRosetta: a script-based interface for implementing molecular modeling algorithms using Rosetta. *Bioinformatics*, **26**, 689–691.
- Chen, J. and Brooks, C.L. (2007) Can molecular dynamics simulations provide high-resolution refinement of protein structure? *Proteins Struct. Funct. Bioinf.*, **67**, 922–930.
- Della Corte, D. *et al.* (2016) Protein structure refinement with adaptively restrained homologous replicas. *Proteins Struct. Funct. Bioinf.*, **84**, 302–313.
- Deng, H. *et al.* (2016) 3DRobot: automated generation of diverse and well-packed protein structure decoys. *Bioinformatics*, **32**, 378–387.
- Feig, M. (2017) Computational protein structure refinement: almost there, yet still so far to go. *Wiley Interdiscipl. Rev. Comput. Mol. Sci.*, **7**, e1307.
- Feig, M. and Mirjalili, V. (2016) Protein structure refinement via molecular-dynamics simulations: what works and what does not? *Proteins Struct. Funct. Bioinf.*, **84**, 282–292.
- Heffernan, R. *et al.* (2015) Improving prediction of secondary structure, local backbone angles, and solvent accessible surface area of proteins by iterative deep learning. *Sci. Rep.*, **5**, 11476.
- Heo, L. and Feig, M. (2018) What makes it difficult to refine protein models further via molecular dynamics simulations? *Proteins Struct. Funct. Bioinf.*, **86**, 177–188.
- Hovan, L. *et al.* (2018) Assessment of the model refinement category in CASP12. *Proteins Struct. Funct. Bioinf.*, **86**, 152–167.
- Ishitani, R. *et al.* (2008) Refinement of comparative models of protein structure by using multicanonical molecular dynamics simulations. *Mol. Simul.*, **34**, 327–336.



- Kabsch, W. and Sander, C. (1983) Dictionary of protein secondary structure: pattern recognition of hydrogen-bonded and geometrical features. *Biopolymers*, **22**, 2577–2637.
- Khatib, F. *et al.* (2011) Algorithm discovery by protein folding game players. *Proc. Natl. Acad. Sci. USA*, **108**, 18949–18953.
- Kim, D.E. *et al.* (2004) Protein structure prediction and analysis using the Robetta server. *Nucleic Acids Res.*, **32**, W526–W531.
- Kryshtafovych, A. *et al.* (2018) Evaluation of the template-based modeling in CASP12. *Proteins Struct. Funct. Bioinf.*, **86**, 321–334.
- Leaver-Fay, A. *et al.* (2011) ROSETTA3: an object-oriented software suite for the simulation and design of macromolecules. *Methods Enzymol.*, **487**, 545.
- Lee, G.R. *et al.* (2016) Effective protein model structure refinement by loop modeling and overall relaxation. *Proteins Struct. Funct. Bioinf.*, **84**, 293–301.
- Lin, M.S. *et al.* (2011) Reliable protein structure refinement using a physical energy function. *J. Computat. Chem.*, **32**, 709–717.
- Mirjalili, V. *et al.* (2014) Physics-based protein structure refinement through multiple molecular dynamics trajectories and structure averaging. *Proteins Struct. Funct. Bioinf.*, **82**, 196–207.
- Modi, V. and Dunbrack, R.L. (2016) Assessment of refinement of template-based models in CASP11. *Proteins Struct. Funct. Bioinf.*, **84**, 260–281.
- Moult, J. *et al.* (2018) Critical assessment of methods of protein structure prediction (CASP)—Round XII. *Proteins: structure. Funct. Bioinf.*, **86**, 7–15.
- Nugent, T. *et al.* (2014) Evaluation of predictions in the CASP10 model refinement category. *Proteins Struct. Funct. Bioinf.*, **82**, 98–111.
- Park, H. *et al.* (2016) CASP11 refinement experiments with ROSETTA. *Proteins Struct. Funct. Bioinf.*, **84**, 314–322.
- Park, H. and Seok, C. (2012) Refinement of unreliable local regions in template-based protein models. *Proteins Struct. Funct. Bioinf.*, **80**, 1974–1986.
- Park, I.-H. *et al.* (2012) Structure refinement of protein low resolution models using the GNEIMO constrained dynamics method. *J. Phys. Chem. B*, **116**, 2365–2375.
- Raval, A. *et al.* (2012) Refinement of protein structure homology models via long, all-atom molecular dynamics simulations. *Proteins Struct. Funct. Bioinf.*, **80**, 2071–2079.
- Rodrigues, J.P. *et al.* (2012) KoBaMIN: a knowledge-based minimization web server for protein structure refinement. *Nucleic Acids Res.*, **40**, W323–W328.
- Rohl, C.A. *et al.* (2004) Protein structure prediction using Rosetta. *Methods Enzymol.*, **383**, 66–93.
- Roy, A. *et al.* (2010) I-TASSER: a unified platform for automated protein structure and function prediction. *Nat. Protoc.*, **5**, 725.
- Summa, C.M. and Levitt, M. (2007) Near-native structure refinement using in vacuo energy minimization. *Proc. Natl. Acad. Sci. USA*, **104**, 3177–3182.
- Tyka, M.D. *et al.* (2011) Alternate states of proteins revealed by detailed energy landscape mapping. *J. Mol. Biol.*, **405**, 607–618.
- Wang, S. *et al.* (2016a) Protein secondary structure prediction using deep convolutional neural fields. *Sci. Rep.*, **6**, 18962.
- Wang, S. *et al.* (2016b) AUC-Maximized deep convolutional neural fields for protein sequence labeling. In: *Joint European Conference on Machine Learning and Knowledge Discovery in Databases*. Springer, pp. 1–16.
- Wildberg, A. *et al.* (2015) Coupling an ensemble of homologues improves refinement of protein homology models. *J. Chem. Theory Comput.*, **11**, 5578–5582.
- Xu, D. and Zhang, Y. (2011) Improving the physical realism and structural accuracy of protein models by a two-step atomic-level energy minimization. *Biophys. J.*, **101**, 2525–2534.
- Zemla, A. (2003) LGA: a method for finding 3D similarities in protein structures. *Nucleic Acids Res.*, **31**, 3370–3374.
- Zhang, J. *et al.* (2011) Atomic-level protein structure refinement using fragment-guided molecular dynamics conformation sampling. *Structure*, **19**, 1784–1795.
- Zhang, Y. (2007) Template-based modeling and free modeling by I-TASSER in CASP7. *Proteins Struct. Funct. Bioinf.*, **69**, 108–117.
- Zhang, Y. (2008) I-TASSER server for protein 3D structure prediction. *BMC Bioinformatics*, **9**, 40.